Advancing Wireless Link Signatures for Location Distinction [*]

Junxing Zhang[†]   Mohammad H. Firooz[‡]   Neal Patwari[‡]   Sneha K. Kasera[†]

[†]School of Computing
University of Utah, Salt Lake City, USA
{junxing, kasera}@cs.utah.edu

[‡]Dept. of Electrical & Computer Engineering
University of Utah, Salt Lake City, USA
{firooz, npatwari}@ece.utah.edu

ABSTRACT

Location distinction is the ability to determine when a device has changed its position. We explore the opportunity to use sophisticated PHY-layer measurements in wireless networking systems for location distinction. We first compare two existing location distinction methods - one based on channel gains of multi-tonal probes, and another on channel impulse response. Next, we combine the benefits of these two methods to develop a new link measurement that we call the complex temporal signature. We use a 2.4 GHz link measurement data set, obtained from CRAWDAD [10], to evaluate the three location distinction methods. We find that the complex temporal signature method performs significantly better compared to the existing methods. We also perform new measurements to understand and model the temporal behavior of link signatures over time. We integrate our model in our location distinction mechanism and significantly reduce the probability of false alarms due to temporal variations of link signatures.

Categories and Subject Descriptors

C.2.3 [**Computer Communication Networks**]: Network Operations - Network Monitoring; C.4 [**Performance of Systems**]: Design Studies

General Terms

Design, Measurement, Performance

Keywords

PHY, Radio Channel, Multipath, Motion Detection

1. INTRODUCTION

Location distinction in a wireless network is the ability to detect, at one or more receivers, when a transmitter has changed its position. Unlike localization or location estimation, location distinction does not attempt to determine where a transmitter is, instead, it detects when that location is different from past locations of the transmitter. Location distinction has the following critical advantages compared to localization: (i) Localization suffers from the inaccuracies caused by the multipath channel. Location distinction can thrive in the multipath channel [11]. (ii) Location distinction is more sensitive to motion. A change in location of less than a meter can be robustly detected by a location distinction algorithm. A localization algorithm may not be able to determine location to within a meter of accuracy, and thus will be unable to reliably detect a meter of motion. (iii) Location distinction needs less coverage. A localization system must have at least three access points or base stations within range of a transmitter in order to locate it. A location distinction algorithm, in many scenarios, can reliably determine a change in position with only one access point or base station in range [11]. Location distinction is critical in many wireless network situations and applications [4, 6, 11]. In surveillance systems, video cameras, laser beams, and pressure detectors are employed to monitor any location change of valuable assets or to tract the movement of a suspicious personnel. In warehouses, radio frequency identification (RFID) tags are widely utilized for inventory and physical security. Here, location distinction is critical in providing a warning so that more resources can be focused on moving objects. In sensor networks, numerous systems have been designed to sense the infrared or acoustic signals from the objects of interest for location or detection purposes. Furthermore, in wireless local area networks, location distinction can be exploited to efficiently locate wireless nodes, detect identity theft, and provide physical evidence.

Location distinction methods based on wireless physical link characteristics, also known as link signatures or fingerprints in the existing literature, are attracting growing attention. In the last few years, researchers have proposed the use of the following three different wireless link signatures.

Received Signal Strength (RSS): RSS is a measurement of the power present in a received radio signal. In [4], Faria *et al* have proposed to measure RSS of signals generated by a host in a WLAN at multiple wireless receivers. A tuple, constructed by aggregating RSS values at different receivers is used as a *signalprint* of the transmitter. Transmitters at

different locations produce different signalprints because of differences in signal decay characteristics between the transmitters and the receivers. Multiple receivers make the RSS based technique more robust by dealing with the temporal variations of RSS and its non-isotropic behavior.

Channel Gains of Multi-tonal Probes: A radio link from a transmitter to a receiver is composed of many paths that are caused by reflections, diffractions, and scattering of radio waves. The multipath characteristics are different at different locations. When a multi-tonal probe is transmitted from a transmitter to a receiver, the different carrier waves experience different gains in the wireless channel. A vector of these channel gains can serve as a link signature [6] because transmitters at different locations, due to unique multipath characteristics, will produce different vectors.

Temporal Channel Impulse Response: The temporal channel impulse response of a link is the superposition of the impulse responses, each one representing a single path in the link multipath. Each impulse is delayed by the path delay, and multiplied by the amplitude and phase of that path. Transmitters at different locations produce different channel impulse responses due to unique multipath characteristics [11].

Being based on the rich multipath characteristics of a wireless link, the last two link signatures are expected to perform better than the simpler RSS-based signature. In fact, Patwari and Kasera [11] have shown that compared to location distinction based on the temporal channel impulse response, the RSS-based method has a consistently lower detection rate and a higher false alarm rate. In this paper, our goal is to explore the opportunity to further advance location distinction techniques in wireless networks. Towards this goal, we first compare the methods based on channel gains of multi-tonal probes and the temporal channel impulse response. We find that when the number of carrier waves is small, the temporal channel impulse response has a higher probability of detection (of location change) but when the number of carrier waves is large, the multi-tonal signature has a higher probability of detection. Next, we use the strengths of these two multipath based methods to develop a new signature that we call a *complex temporal signature.* We use a 2.4 GHz channel measurement data set, obtained from CRAWDAD [10], to evaluate the two existing multipath based, and our new, link signatures. We find that the complex temporal method exhibits the highest performance in terms of high detection rate and low false alarm rate.

None of the past research on location distinction has evaluated the temporal behavior of link signatures. A location distinction mechanism that does not consider the temporal changes in link behavior can increase the probability of false alarms. In this paper, we use measurements of the complex temporal signatures to develop and model temporal profiles of links. We model the temporal behavior using a K-state Markov chain such that link signatures measured in one state are very similar to each other, while those measured belonging to different states of the Markov chain are noticeably different from each other. We integrate our Markov model in our location distinction mechanism. We find that our integrated location distinction significantly reduces the probability of false alarms.

The rest of this paper is organized as follows. The two existing multipath-based link signatures are described and compared in Section 2. In Section 3, we refine the existing methods to develop a new link signature. An framework for evaluating location distinction methods is outlined in Section 4. We extensively evaluate all the link signatures in Section 5. We present our temporal behavior measurements and results in Section 6. Section 7 summarizes the related work on wireless link signatures. We conclude the paper and indicate directions for future work in Section 8.

2. A COMPARISON OF MULTIPATH-BASED LINK SIGNATURES

In this section, we describe and qualitatively compare two existing multipath-based link signatures and metrics for location distinction. We start with an overview of multipath channel response and then describe the multiple tone and the temporal channel impulse response methods. We define the link signature and the location distinction evaluation metric under each method. We end this section by comparing the two methods and discussing the benefits of each method.

2.1 Multipath Channel Response

Both link signatures in [6] and [11] are functions of the multipath channel response. The wireless channel from the transmitter to the receiver consists of multiple paths caused by reflections, diffractions, and scattering of the radio waves. Essentially, the received signal contains multiple time-delayed, attenuated, and phase-shifted copies of the original signal. Because these multipath characteristics in the channel response change considerably at different locations, measurements of the channel are a good "signature" or "fingerprint" of the link and can be used for identification purposes.

The impulse response of a time-variant multi-path fading channel can be written as follows:

$$h(t,\tau) = \sum_{l=1}^{L(t)} \alpha_l(t)e^{j\phi_l(t)}\delta(\tau - \tau_l(t)) \tag{1}$$

where $h(t,\tau)$ is the impulse response of the channel at time t to a signal at time $t - \tau$. It is assumed that there are $L(t)$ paths between the transmitter and receiver, and $\tau_l(t)$ is the delay of the lth path, $\alpha_l(t)$ is its gain, and $\phi_l(t)$ is its phase shift. In a short period of time, for example, for a packet duration, it is reasonable to consider the channel as a time-invariant filter with the following impulse response:

$$h(\tau) = \sum_{l=1}^{L} \alpha_l e^{j\phi_l}\delta(\tau - \tau_l) \tag{2}$$

When channel response is represented in the time domain as $h(t)$, it is called the *channel impulse response* (CIR). Its Fourier transform $H(f) = \mathfrak{F}\{h(\tau)\}$ represents the channel response in the frequency domain, and is the *channel frequency response.* By sending s(t) through the channel, the receiver receives:

$$r(t) = s(t) * h(t) = \sum_{l=1}^{L} \alpha_l e^{j\phi_l}s(t - \tau_l) \tag{3}$$

The received signal is the convolution of the sent signal and the channel response in the time domain. In the frequency domain, it is simply the product of the transmitted signal and the channel frequency response.

$$R(f) = S(f)H(f) \tag{4}$$

In order to create a link signature independent of the transmitted signal $S(f)$, the channel response must be recovered from the received signal. One of the following two methods can be used,

$$H(f) = \frac{1}{\mathcal{P}_s}S^*(f)R(f) = \frac{1}{\mathcal{P}_s}|S(f)|^2 H(f) \qquad (5)$$

$$H(f) = \frac{R(f)}{S(f)} \qquad (6)$$

where $\mathcal{P}_s$ is the power of the sent signal inside the band. Note that the first expression assumes that $|S(f)|^2$ is approximately constant for the given modulation scheme, and the second expression assumes that $S(f)$ is non-zero in the band of interest. The recovered channel response can be represented in either the time domain as $h(t)$ or in the frequency domain as $H(f)$. Various functions of either could be used to represent the channel response. There are also varied signals that can be used to measure the channel response. These factors may lead to a variety of multipath channel-based link signatures.

2.2 Multiple Tone Probing

In [6], multiple tone probing is used to generate a multipath channel-based link signature. The critical feature of this method is that it measures frequency response, and in particular, complex attenuation at multiple frequencies. We first show how this method measures samples of the complex frequency response of the channel, and then relate how the similarity of a signature and a history of past measurements is quantified.

2.2.1 Signature

In this method K carrier waves are simultaneously transmitted to the receiver. The transmitted signal in the time domain and frequency domain are given as,

$$s(t) = \sum_{\kappa=1}^{K} e^{j2\pi f_\kappa t} \qquad (7)$$

$$S(f) = \sum_{\kappa=1}^{K} \delta(f - f_\kappa) \qquad (8)$$

where f_κ is the carrier frequency of the κth carrier wave. Note that carrier frequencies f_κ should be separated by an amount greater than channel coherence bandwidth. Each carrier wave is attenuated by the channel complex gain at its center frequency, as indicated by (4). Thus the received signal is given in the frequency domain as,

$$R(f) = \sum_{\kappa=1}^{K} H(f_\kappa)\delta(f - f_\kappa) \qquad (9)$$

where $H(f_\kappa)$ is the complex gain at f_κ.

The vector of these gains $\{H(f_\kappa)\}$ is used as the multiple tone signature. The nth recorded multiple tone signature of the link between transmitter i and receiver j is

$$\mathbf{h}_{i,j}^{(n)} = [H^{(n)}(f_1), \ldots, H^{(n)}(f_K)]^T. \qquad (10)$$

Although a special multiple tone signal is used in [6], we note that the identical channel frequency response could be measured with an arbitrary signal if $S(f)$ was known at the receiver, because complex channel gains $\{H(f_\kappa)\}$ could be

calculated using (6) at any frequencies f_κ for which $S(f_\kappa) \neq 0$.

2.2.2 Metric

In the multiple tone probing method of [6], the Nth multiple tone signature $\mathbf{h}^{(N)}$ is compared with each previously measured signature in the history $\mathcal{H}_{i,j}$ using a measure called the correlation statistic. The average correlation statistic is given by

$$sigEval(\mathbf{h}^{(N)}, \mathcal{H}_{i,j}) = \frac{1}{N-1}\sum_{n=1}^{N-1}|T^{(n)}| \qquad (11)$$

where $T^{(n)}$ is the correlation of the nth and the Nth measurements,

$$T^{(n)} = \frac{\sum_\kappa H^{(n)}(f_\kappa)H^{(N)}(f_\kappa)^*}{K\gamma_A^{(n)}} \qquad (12)$$

where $\gamma_A^{(n)}$ is average squared magnitude of the elements of $\mathbf{h}_{i,j}^{(n)}$: $\gamma_A^{(n)} = \|\mathbf{h}_{i,j}^{(n)}\|^2/K$.

The correlation statistic in (11) is a measure of *similarity*. If the correlation is low, then the Nth signature is very different from those in the history. In contrast, if the correlation is high, then the new measurement is very similar to those in the history.

2.3 Temporal CIR Signature

In the temporal link signature method in [11], the link signature is measured in the time domain. One main difference between this method and the multiple tone probing method is its estimation of the impulse response as a function of time delay, and in particular, the magnitude of the impulse response. We first show how the temporal link signature is computed, and then describe the metric used to quantify its distances from a history of past measurements.

2.3.1 Signature

In [11], an unmodulated direct-sequence spread-spectrum (DS-SS) signal is sent from a transmitter. In other words, a known pseudo-noise (PN) code signal is transmitted as $s(t)$. Because $S(f)$ of a PN code signal is approximately flat within the band, the channel response $H(f)$ is recovered from (5).

The temporal impulse response $h(t)$ is then obtained by calculating $\mathfrak{F}^{-1}\{H(f)\}$, the inverse Fourier transform of $H(f)$. Noting that random phase shifts occur between measurements of $h(t)$, the link signature is taken in [11] to be the magnitude of the temporal impulse response. The nth sampled link signature measurement of the link between transmitter i and receiver j is then,

$$\mathbf{h}_{i,j}^{(n)} = [|h^{(n)}(0)|, \ldots, |h^{(n)}(ST_r)|]^T \qquad (13)$$

where T_r is the sampling interval at the receiver and $S + 1$ is the number of samples.

Although a PN code signal is used in [11], again, an arbitrary transmitted signal with $S(f)$ known at the receiver, could be used to estimate $H(f)$ and thus $h(t)$.

2.3.2 Metric

In the temporal link signature, the difference between the Nth signature $\mathbf{h}^{(N)}$ and those in the history $\mathcal{H}_{i,j}$ is given as the minimum normalized Euclidean distance between the

new signature and any signature in the history set. The definition is given in the Equation (14) below.

$$sigEval(\mathbf{h}^{(N)}, \mathcal{H}_{i,j}) = \frac{1}{\sigma_{i,j}} \min_{\mathbf{h} \in \mathcal{H}_{i,j}} \|\mathbf{h} - \mathbf{h}^{(N)}\|_{\ell 2} \qquad (14)$$

where $\sigma_{i,j}$ is the normalization factor,

$$\sigma_{i,j} = \frac{1}{(N-1)(N-2)} \sum_{\mathbf{g}, \mathbf{h} \in \mathcal{H}_{i,j}} \|\mathbf{h} - \mathbf{g}\|_{\ell 2} \qquad (15)$$

Note that the distance in (14) is divided by the average distance between historic signatures $\sigma_{i,j}$ as defined in (15) in order to normalize to the normal temporal variations in the radio channel.

The metric in (14) indicates the *difference* between a new measurement and the stored history measurements. When $sigEval(\mathbf{h}^{(N)}, \mathcal{H}_{i,j})$ is low, it indicates that the new measurement is very similar to the history; when it is high, it is very different. Both methods [11] and [6] quantify relationships between measurements, but are opposite in the interpretation of the metric. This will be discussed again in Section 4.

2.4 Discussion

The link signatures in the multiple tone probing method and in the temporal link signature method both make measurements of the multipath channel and use them to quantitatively identify a link. The work of [6] and [11] use particular signals to enable channel measurement, but both can be used with arbitrary transmitted signals. Thus it is of clear interest to compare the two methods prior to making improvements to them in Section 3. While a quantitative comparison is made in Section 5, this section discusses qualitatively the merits of the two approaches.

The temporal link signature measures a band-limited version of the channel impulse response in (2). In the time domain, each multipath contributes an impulse at a particular time delay. If a change in the channel occurs, for example, because of a person walking by, it is likely that the change occurs to a single path. Because multiple paths are largely orthogonal in the time domain, a change in the phase of one path can affect only a small portion of the time-delayed samples, and the feature vector remains mostly stationary over time.

However, the channel frequency response is sensitive to each multipath. Since an impulse in the time domain is a constant in the frequency domain, a change to a single path may change the entire multiple tone link signature. For this reason, a temporal signature can be more robust against small changes in multipath. Note that if the transmitter moves position, that all multipath are likely to change, and both temporal and multiple tone link signatures will change dramatically.

Importantly, the multiple tone link signature is a complex measurement, while the temporal link signature is a real-valued measurement. The inclusion of phase information in the multiple tone signature effectively increases the richness of the measurement space. The temporal link signature, with only magnitude information, does not retain some identifiable information about a link captured by the channel phase response, and thus we would expect it to lose some ability to uniquely identify links.

3. INNOVATIVE METHODS

In this section we propose improvements to the link signatures described in Section 2. First, for the multiple tone link signature, we propose a new metric which improves its robustness to changing received powers. Second, we present a new superior link signature method which we call the *complex temporal link signature*, that combines the strength of the two signatures described in Section 2, and show that a simple metric is robust to uninformative, random phase shifts and can thus accurately quantify the distance between two measured link signatures.

3.1 Refined Metric for Multiple Tone Signatures

The refined metric for the multiple tone signature is inspired by a close study of the original correlation statistic. Our evaluation in Section 5.1.1 demonstrates that this new metric indeed improves the signature performance.

3.1.1 Normalized Metric

We denote this new metric as the *normalized metric*. We can view the normalized metric as the result of normalizing each multiple tone signature to its magnitude before the calculation of the correlation statistic. Specifically,

$$\tilde{\mathbf{h}}_{i,j}^{(n)} = \frac{\mathbf{h}_{i,j}^{(n)}}{\|\mathbf{h}_{i,j}^{(n)}\|} \qquad (16)$$

Plugging this into (12), the new $T^{(n)}$ is given by

$$T^{(n)} = \frac{\sum_{\kappa} H^{(n)}(f_\kappa) H^{(N)}(f_\kappa)^*}{\|\mathbf{h}_{i,j}^{(n)}\| \|\mathbf{h}^{(N)}\|}. \qquad (17)$$

This is equivalent to the following,

$$T^{(n)} = \frac{1}{K} \sum_{\kappa} \frac{H^{(n)}(f_\kappa)}{\sqrt{\gamma_A^{(n)}}} \frac{H^{(N)}(f_\kappa)^*}{\sqrt{\gamma_E}} \qquad (18)$$

where $\gamma_E = \frac{1}{K} \|\mathbf{h}^{(N)}\|^2$. This representation of (17) shows that each channel frequency response is normalized to the square root of its average power.

The correlation statistic, given by (11), is then used to quantify the difference between the Nth link signature and the recorded history.

3.1.2 Discussion

The new normalized metric allows the multiple tone probing method to be robust to differences in the received power between the new channel signature $\mathbf{h}^{(N)}$ and the signatures in the history. In the original metric in (12), the statistic T^n is normalized only to the power in signature $\mathbf{h}_{i,j}^{(n)}$ in the history, not to the power of the new signature $\mathbf{h}^{(N)}$.

Consider the scenario in which the new signature $\mathbf{h}^{(N)}$ has a significantly larger magnitude because it is from another transmitter closer to the receiver than the original transmitter. In this case, the original T^n will have a very high variance, and even though it would have zero mean, the correlation statistic may often exceed the threshold due to the high variance. This would lead to frequent missed detections, since we distinguish different locations based on low correlation. In the new definition of T^n in (17), another nearby transmitter would not increase the variance of

T^n, and thus we would consistently measure low correlation statistic.

3.2 Complex Temporal Signature

Finally, we present a new link signature method we call the complex temporal signature method, which combines the best features of both the temporal link signature method and the multiple tone probing method. As mentioned in Section 2.4:

- The temporal link signature has the advantage of operating in the time domain which de-correlates multipath at different delays;

- The multiple tone link signature has the advantage of using a complex-valued signature which preserves phase information

This section presents the complex temporal signature, which incorporates phase information into a time-domain channel representation. We discuss the problem of random phase shifts, which are a result of clock and frequency shifts, rather than changes in the channel. Finally, we show that a new ϕ_2 difference can be used to eliminate the effects of random phase shifts when quantifying distance between complex temporal link signatures.

3.2.1 Enhance The Signature

As indicated, we change the definition of the link signature to be the vector of the complex value of the channel impulse response,

$$\mathbf{h}_{i,j}^{(n)} = [h^{(n)}(0), \ldots, h^{(n)}(ST_r)]^T, \qquad (19)$$

where, again, T_r is the sampling rate and $S+1$ is the number of samples. This signature is the inverse Fourier transform of $H(f)$, which is calculated from (5). Compared to (13), the magnitude of each gain is not taken, so the complex link signature retains phase information in a manner similar to the multiple tone link signature.

3.2.2 Issue: Phase Changes

As phase changes are preserved in the complex temporal link signature, phase differences between two link signatures can be used as part of the metric which quantifies the difference between them. However, this can be problematic because some phase changes in the link signature have nothing to do with any changes in the link. The authors in [6] have noted that, although they tried to minimize the temporal variations of link signatures by conducting experiments during a time of no activity in the building, they encountered difficulty discriminating between channel response phase and oscillator drift. They worked around the problem by comparing the magnitude of the gain, but we want to offer an solution here.

In particular, in typical wireless communications links, the lack of time and frequency synchronization causes phase changes between link signature measurements. Recall that the phase of the received signal is $\varphi + 2\pi f t$, where φ is the initial phase of the transmitted signal. If the clock of the transmitter is not synchronized very well with that of the receiver, the phase of the received signal will change by $2\pi f \Delta t$, where Δt is the time offset between the two clocks. This $2\pi f \Delta t$ will be an unknown phase at the transmitter. Another cause of phase change is the fact that two wireless devices (transmitter and receiver) will always have slightly different carrier frequencies f_{Tx} and f_{Rx}. In this case, the phase difference between two measurements will be $2\pi (f_{Tx} - f_{Rx})t$. Even the most accurate clocks will have a phase that cycles many times per second, and any given measurement will have a random phase.

The random phase shift due to lack of synchronization affects the entire duration of the link signature. In other words, in a completely static channel, if the first measured complex temporal link signature was $\mathbf{h}$, then the next complex temporal link signature would be measured as $e^{j\phi}\mathbf{h}$. An example from measurements in Figure 1 shows these changing phase shifts among five measured complex temporal link signatures as rotations in the complex plane.
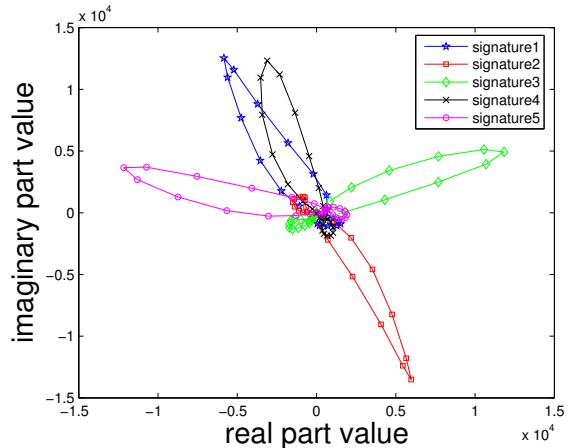

Figure 1: Phase shifts in signatures of a sample link

3.2.3 Calculating Distance Among Phase Shift

Because these phase shifts ϕ are not due to the channel, we must ignore them when calculating the difference between signatures. Intuitively, we should determine the phase shift ϕ, and then multiply the shifted complex link signature by $e^{-\phi}$, essentially, rotating the two signatures to align in the complex phase plane, and then calculate their difference. In this section, we introduce a ϕ_2 difference to perform this alignment and measure the distance between two signatures without being affected by random phase shifts.

We intuitively understand that the proper difference as one involving a rotation of one link signature to align with the other, prior to calculating a distance. Consider this intuitive difference given two complex temporal link signatures $\mathbf{h}$ and $\mathbf{g}$. We represent this shift-removed difference with a new ϕ_2 difference. It is defined as $\|\mathbf{g} - \mathbf{h}\|_{\phi2} = \min_{\phi \in (0,2\pi)} \|\mathbf{g}e^{j\phi} - \mathbf{h}\|_{\ell 2}$, where $\|\cdot\|_{\ell 2}$ indicates the Euclidean distance. Simplifying, we have:

$$\begin{aligned}
\|\mathbf{g} - \mathbf{h}\|_{\phi2}^2 &= \min_{\phi \in (0,2\pi)} \|\mathbf{g}e^{j\phi} - \mathbf{h}\|_{\ell 2}^2 \\
&= \min_{\phi \in (0,2\pi)} (\mathbf{g}e^{j\phi} - \mathbf{h})^* (\mathbf{g}e^{j\phi} - \mathbf{h}) \\
&= \|\mathbf{g}\|^2 + \|\mathbf{h}\|^2 - 2 \max_{\phi \in (0,2\pi)} \Re(\mathbf{g}^* e^{j\phi} \mathbf{h}) \\
&= \|\mathbf{g}\|^2 + \|\mathbf{h}\|^2 - 2\|\mathbf{g}^* \mathbf{h}\| \qquad (20)
\end{aligned}$$

where the function $\Re()$ returns the real part of a complex number. This derivation shows that the ϕ_2 difference, which minimizes the random phase shift between two measure-

ments before calculating distance, can be efficiently and explicitly calculated using simple vector operations.

4. FRAMEWORK FOR LOCATION DISTINCTION

In this section, we outline a step-by-step decision and estimation framework for using link signatures for location distinction. This framework is similar to the one used by Patwari *et al* in [11]. Different signatures and metrics introduced in the previous two sections can be fitted into this framework for performance evaluation.

1. For a given transmitter i and a receiver j where $i \neq j$, a history of $N-1$ link signatures is measured and stored as $\mathcal{H}_{i,j} = \{\mathbf{h}_{i,j}^{(n)}\}_{n=1}^{N-1}$.

2. The Nth signature $\mathbf{h}^{(N)}$ at j from an unknown transmitter in the neighborhood of j is then taken, and an evaluation criterion $e_{i,j} = sigEval(\mathbf{h}^{(N)}, \mathcal{H}_{i,j})$ is computed. The function $sigEval()$ uses different signature metrics to compare the Nth measurement against the history. These metrics have been defined in the previous two sections.

3. Next, $e_{i,j}$ is compared to a threshold γ. When $e_{i,j}$ satisfies certain conditional relationship with γ, the new signature is determined to be from a different transmitter and a location change is detected. The conditional relationship is either *greater than* or *less than*, depending on the evaluation metric in use. For the correlation metrics, it is less than. For the distance metrics, it is greater than.

4. When $e_{i,j}$ does not satisfy certain conditional relationship with γ, the new signature is determined to be from the same transmitter, i.e. $\mathbf{h}^{(N)} = \mathbf{h}_{i,j}^{(N)}$, and we include it in $\mathcal{H}_{i,j}$. For constant memory usage, the oldest measurement in $\mathcal{H}_{i,j}$ is then discarded. The algorithm returns to step 2 until enough measurements have been collected.

5. For performance evaluation, we wish to find out the probability of false alarm P_{FA} and probability of detection P_D of the different location distinction methods. We first define the null and alternate hypotheses: $\mathbb{H}_0$ and $\mathbb{H}_1$.

$$\mathbb{H}_0: \qquad e_{i,j} = e_{i,j}^{(N)}$$
$$\mathbb{H}_1: \qquad e_{i,j} = e_{i-i',j}$$

where $e_{i,j}^{(N)}$ is the difference between the Nth measurement of a link and the history of the same link and $e_{i-i',j}$ is the difference between the Nth measurement of a link and the history of a different link. We treat $e_{i,j}$ as a random variable and denote its conditional density functions under the above two events as $f_{e_{i,j}}(x|\mathbb{H}_0)$ and $f_{e_{i,j}}(x|\mathbb{H}_1)$. We calculate P_{FA} and P_D as given in [5]:

$$P_{FA} = \int_{x=\gamma}^{\infty} f_{e_{i,j}}(x|\mathbb{H}_0)dx$$
$$P_D = \int_{x=\gamma}^{\infty} f_{e_{i,j}}(x|\mathbb{H}_1)dx$$

The above framework uses a single receiver. We can also extend it to a multi-receiver collaborative framework. For the multi-receiver case, we need to run the first step at each receiver, and calculate the mean $e_{i,j}$ in the second step. Because we use similar multi-receiver framework as defined in our previous paper[11], we leave out details here for brevity. However, we will present the results from the multi-receiver collaborative framework in Section 5.

5. QUANTITATIVE COMPARISONS OF LINK SIGNATURES

In this section, we compare the performances of multiple tone probing, temporal channel impulse response, and the complex temporal link signatures using a data set of measured radio channels, obtained from CRAWDAD [10]. These measurements of this data set are reported to have been recorded in an office environment among a set of 44 different node locations. The data set contains five measurements of the channel for each pair of the 44 nodes. The first four measurements are used in these evaluations to form the channel history, while the fifth is used as a test measurement. In other words, $N = 5$ and the history is composed of measurements $n = 1, \ldots, 4$. We use the data set to compare location distinction both when a transmitter has actually changed its position, and when it has not. For the case when the transmitter has not moved, we test the fifth measurement on link (i, j) against the measurement history of this link. For the case when the transmitter *has* moved, we consider all triplets (i, k, j) with $i \neq k \neq j$, where k is the new transmitter location, and (i, j) is the original link. For each triple, the fifth measurement in the new link (k, j) is compared with the history of the link (i, j). As described in Section 4, we quantify the performance of each link signature by computing the probability of detection and the probability of false alarm. We use the receiver operating characteristic (ROC) plot, that shows how the probability of detection varies with the probability of false alarm, to display the performance of each link signature.

5.1 Direct Measurement Evaluation

5.1.1 Multiple Tone Performance

We first evaluate the performance of the multiple tone probing method with both the original and the normalized metric using the measurement data set. When the correlation statistic is measured for a transmitter that has not changed location compared the history ($\mathbb{H}_0$) it is referred to as an *auto-correlation* statistic. In contrast, when the correlation statistic is measured for a transmitter at a different location ($\mathbb{H}_1$) it is referred to as a *cross-correlation* statistic.

The cross-correlation values of the original metric motivate our new metric. Using the original metric of (12), these cross-correlation values are very high in magnitude, as high as 70. Comparatively, using the normalized metric in (17), the cross-correlation values are reliably below 1. This experimental result validates the discussion in Section 3.1.2 which motivated our normalized metric.

The ROC curves comparing the two metrics are shown in Figure 2. They show that without the normalized metric, the multiple tone method must accept a very high probability of false alarm in order to perform location distinction. Yet with the normalized metric, multiple tone probing performs well even at low probability of false alarm.
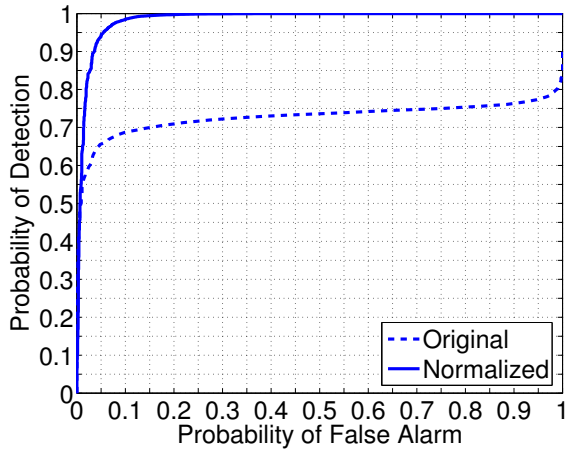
Figure 2: ROC curves of comparing performance of original and the normalized metrics in the multiple tone probing method.

5.1.2 Comparison of Multiple Tone and Temporal Link Signatures

Next, in this section, we compare the temporal link signature with the multiple tone probing link signature (using the normalized metric). Figure 3 shows the comparison results. Both ROC curves of the temporal link signature and the multiple tone signature are displayed. Since it is possible to change the number of tones K used by the multiple tone probing method, more than one multiple tone curve is depicted, each with the K indicated. The result shows the general improvement in the multiple tone probing method as K increases.

The temporal link signature has better detection performance than the multiple tone probing method when K is low, but performs worse than the multiple tone probing when $K = 25$ and 50. The trend of Figure 3 suggests increasing tone numbers improves the performance of the multiple tone signature. When the tone number increases from 3, 5, 7, 10, 15, until 25, we see better and better ROC curves. There are, however, diminishing returns as K is increased. This situation is related to the *coherence bandwidth*, because the K tones are taken from a constant bandwidth. As K increases, the spacing between f_κ decreases. When different tones are not separated enough, the channel gains $\{H(f_\kappa)\}_\kappa$ will be correlated and thus including them in the signature will not provide as much distinction capability. The original Multiple Tone Probing explicitly requires the tones to be separated by an amount greater than the channel coherence bandwidth [6]. It also explains why the 25-tone signature performs almost as well as the 50-tone signature. The latter signature may have tones too closely spaced that don't actually improve performance.

5.1.3 Complex Temporal Performance

Next, we evaluate the new complex temporal signature method described in Section 3.2. Again, we compare the performance of the three methods, multiple tone probing (with normalized metric), temporal link signature, and complex temporal link signature, using ROC curves. These ROC curves are shown in Figure 4. In Figure 4(a), the curves look very close because the full range of both P_{FA} and P_D are
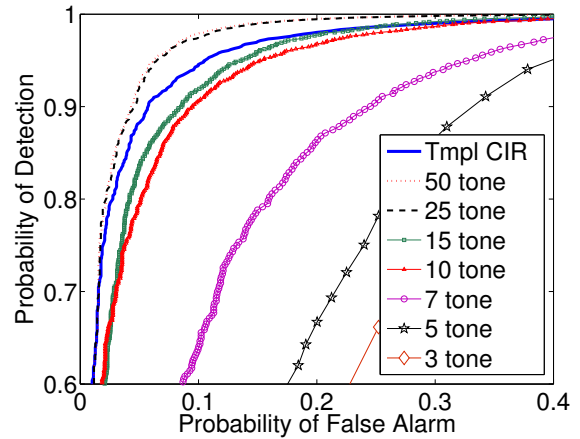

Figure 3: Comparison of the temporal link signature with the normalized multiple tone signatures of various tone numbers

P_{FA} points	0.04	0.06	0.08
Temporal P_D	0.8517	0.9066	0.9285
50-Tone P_D	0.8888	0.9486	0.9651
Complex P_D	0.9467	0.9633	0.9744

Table 1: Compare detection rates of three best signatures under given false alarm rates

given. Figure 4(b) zooms in to the relevant low P_{FA} and high P_D regions, to provide more information.

To provide a specific quantitative comparison at some prospective operating points, we set particular values of the false alarm rate and show the possible detection performance of the three methods in Table 1.

In comparison, the complex temporal link signature significantly outperforms both the multiple tone probing and temporal link signature methods. The 'missed detection' rate of the complex temporal link signature method, that is, $1 - P_D$, is cut in third compared to the temporal link signature method, and cut in about half compared to the 50-tone probing method. The complex temporal link signature performs especially well when false alarm rates are low. As an exception, the multiple tone probing has a very slightly higher detection rate, as barely seen in Figure 4(a), than the complex temporal link signature when the false alarm rate becomes higher than 15%. It appears that certain phase changes in the measurements cannot be detected by the complex temporal link signature. This situation however is very rare in our measurements and it does not occur when measurements from multiple receivers are used as described in the next subsection.

5.2 Multiple Receiver Performance

In both [4] and [11], the robustness of the location distinction methods is higher when multiple receivers are used to jointly detect a change in transmitter location. We now perform a similar evaluation of a multiple-receiver framework for both the improved multiple tone signature and the complex temporal signature.

For the multiple receiver framework, we consider all possible combinations of transmitters and receivers. Let there be n devices (n=44 in the experimental set up) and m re-
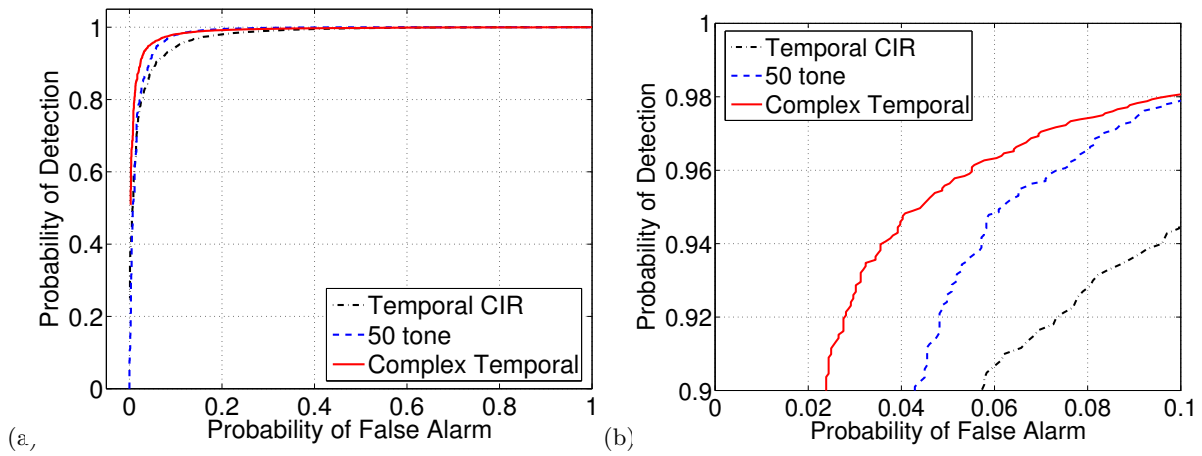
Figure 4: Comparison of the complex temporal signature, temporal link signature, and multiple tone probing method with normalized metric, showing (a) ROC curves, and (b) zoom-in of ROC curves.
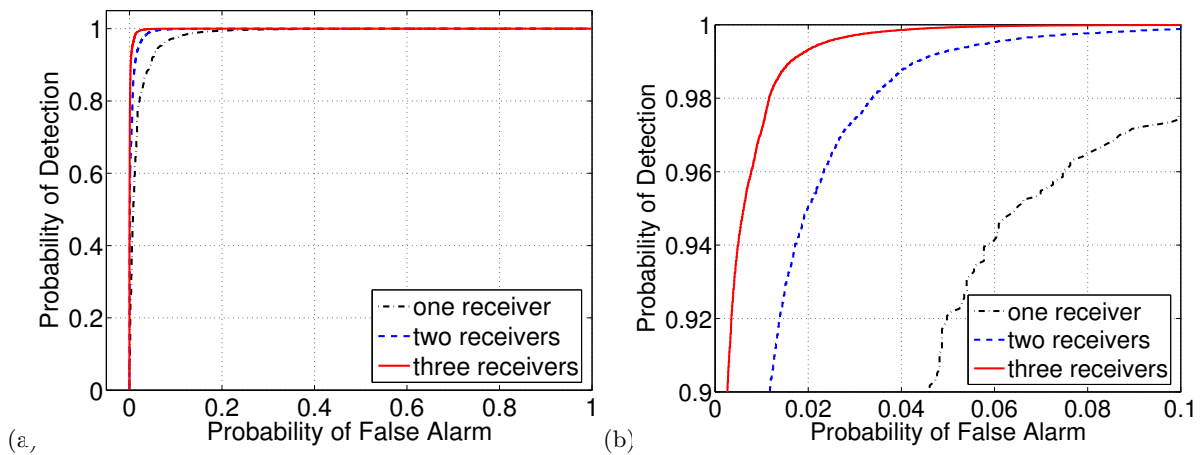

Figure 5: The multiple receiver improvement of the normalized multiple tone signature. (a) ROC curve and (b) larger view of $0 \leq P_{FA} \leq 0.1$ and $0.9 \leq P_D \leq 1$.
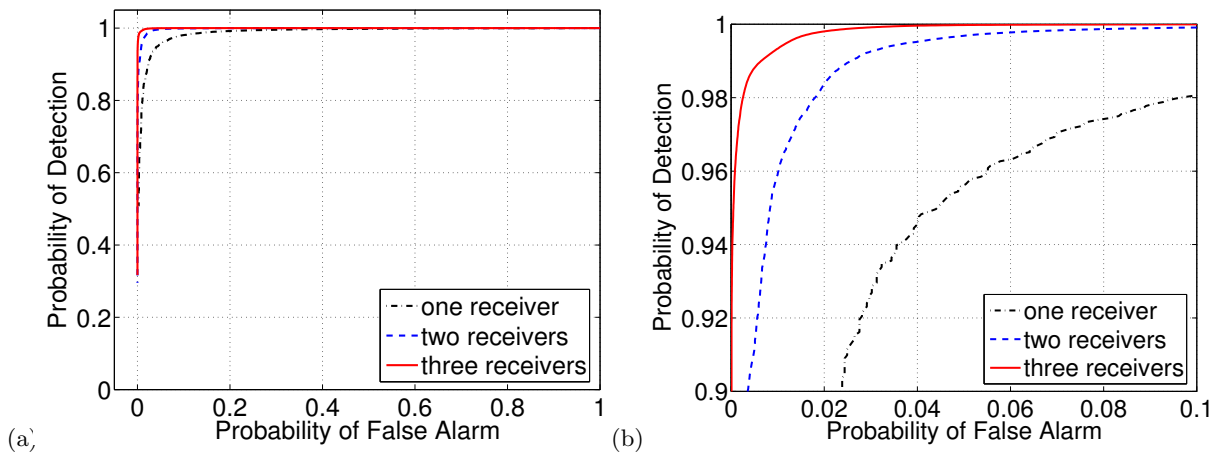

Figure 6: The multiple receiver improvement of the complex temporal signature. (a) ROC curve and (b) larger view of $0 \leq P_{FA} \leq 0.1$ and $0.9 \leq P_D \leq 1$.

ceivers in the joint detection setup (m=2, 3 in this set up). We choose m receivers out of n devices, choose one transmitter out of the $n-m$ non-receivers, and one other transmitter out of the remaining $n - m - 1$ devices. There are a total of $\binom{n}{m}(n-m)(n-m-1)$ possibilities. For these possible transmitter/receiver setups, we calculate the false alarm probability P_{FA} and the detection probability P_D.

5.2.1 Improved Multiple Tone

The ROC curves of the two-receiver and three-receiver algorithms are generated for the improved multiple tone signature. They are compared with the one-receiver curve in Figure 5. The overall ROC plot shows the improving trend of the performance from the one-receiver to the two-receiver and then to the three-receiver. The larger view shows the first improvement is bigger than the second improvement.

5.2.2 Complex Temporal

Next, Figure 6 shows the changes in the performance of the complex temporal signature due to the increased number of receivers. The trend is that performance improves with the number of receivers and the difference in improvement increments are consistent with the previous figure. When comparing two figures, especially comparing the larger views of the two figures, it is clear that the complex temporal signature outperforms the multiple tone probing method consistently in all cases.

6. TEMPORAL BEHAVIOR OF LINK SIGNATURES

So far, we have focused mostly on the spatial behavior of the wireless links. Due to external factors such as movement of people and that of objects, especially metallic objects, the multipath characteristics of a link can change with time. A link can thus be in different distinct states. A location distinction mechanism that does not consider the temporal changes in link behavior can significantly increase the probability of false alarms. In order to build a comprehensive and accurate location distinction mechanism we must carefully consider the changes in the temporal behavior of links. Unfortunately, the measurement data that we have used in the previous sections [10] only contains a history of four signatures per link that were obtained in close time proximity. Motivated by the lack of data on the temporal behavior of link signatures, we perform a measurement campaign to obtain new data and model the temporal behavior of wireless link signatures. We then integrate our model in our location distinction mechanism. In this section, we first describe our measurement campaign. We measure the complex temporal link signature only because, as shown in Section 5.1.3, it performs the best among the three signatures we evaluate in this paper. Next, we develop a Markov model from the measurement data. Last, we evaluate the performance of our integrated location distinction mechanism.

6.1 Measurement Campaign

We measure the temporal behavior of wireless links in a typical university building that houses department offices, research labs, classrooms, conference rooms, and other educational facilities. We use a direct-sequence spread-spectrum (DS-SS) transmitter and receiver (Sigtek model ST-515) for our measurement campaign. The transmitter sends a DS-SS

signal, an unmodulated pseudo noise signal with a 40 MHz chip rate, a 1024 code-length, and a central frequency of 2443 MHz. The receiver recovers channel responses and records response vectors comprising 600 complex temporal impulse responses. Each impulse response is a vector of 100 complex numbers. We choose four different transmitter/receiver location pairs for this campaign. In the first pair, the receiver is in a large research lab and the transmitter is located in a nearby room (LOC B). Both rooms are adjacent to a hallway. The same research lab holds the receiver in the second pair, but the transmitter is instead placed in a small office that is separated from the hallways by other rooms (LOC A). In the third pairs, the receiver is in a small research lab and the transmitter is in a conference room (LOC C). Finally, we have the transmitter and receiver placed on two different floors (LOC D). The two locations are horizontally close but vertically separated by a combination of floor and ceiling. Our choice of transmitter and receiver locations allows us to obtain data under varying conditions especially in terms of varying movement of objects.
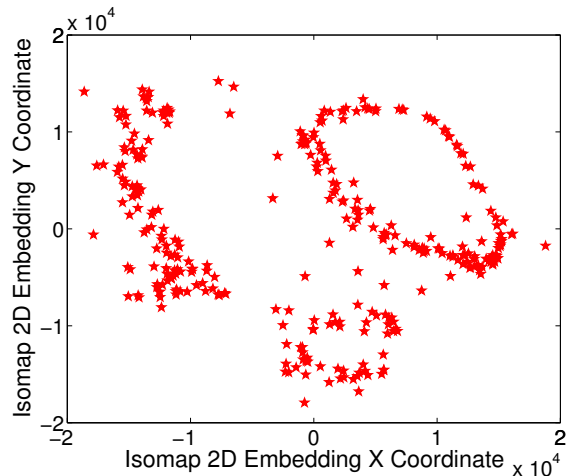
6.2 Models

Figure 7: Isomap 2D embedding coordinates for a set of link signatures over time.

Analysis of our measurement sets show that the link signatures measured on a link change over time, and that these different measurements appear to fall into different states. Within a small number of states, these link signatures are very similar to each other, and each state produces noticeably different link signatures.

In order to quantify the inter-state and intra-state distances, we use non-linear dimensionality reduction[1] to reduce the 100 dimension vectors to just 1-2 dimensions. In particular, we apply the well-known Isomap algorithm of Tenenbaum *et al* [12] to the complex link signature measurements. As an example, we plot in Figure 7 a 2-D embedding of one set of 333 complex link signature measurements. The results clearly show three separate groups of measured data[2]. We see that within each group, measured

---

[1]Non-linear dimensionality reduction is generally used in statistics to visualize high dimensional data.

[2]Note that this is our only data set that contains three states.

link signatures vary in a cyclical manner. In different groups, measured link signatures are noticeably different, and thus appear separately.

6.2.1 Markov model

We model the groups of link signatures as a K-state Markov chain where each group is considered to be a state of the Markov chain. Then, we use the following procedure to calculate the transition probabilities between states. This procedure uses the 1-D embedding of the Isomap algorithm. Figure 8 shows the temporal behavior of the 1-D embedding for data set from LOC A. This figure indicates a strong periodic sinusoid-like temporal pattern. While the channel is in different states, the signal has different amplitudes. In fact, this signal is like an amplitude modulation (AM) signal, a sinusoid which carries information as its amplitude.
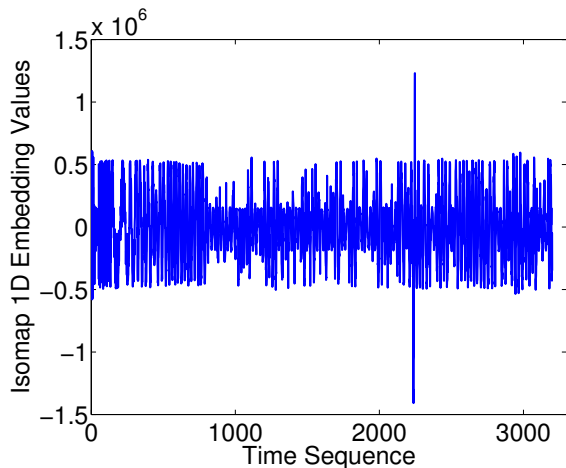

Figure 8: Isomap 1D embedding coordinates for a set of link signatures over time.

We use an AM demodulator to capture the envelope of the pattern. In the AM demodulator, the squared one-dimensional embedding signal is passed to a low-pass filter to track the 'envelope' or amplitude of the 1-D embedding signal. The envelope is shown in Figure 9 together with the squared embedding values.

Figure 9 quantifies when the Markov chain switches between states. Since there are two states (LOC A data set), we detect a transition when the envelope exceeds a threshold. Each time that it changes from below to above, or above to below the threshold, we have a state change. From the total number of state changes, and the number of times we are in a state, we calculate the state transition probabilities and the limiting probabilities of the Markov chain. For the four measurement sets, one each from the four links (LOC A - LOC D), we list these probabilities in Table 2[3].

Given the Markov chain representation of the temporal behavior of link signatures, we evaluate the following two distinct types of false alarms.

1. *Same-State False Alarm (SSFA)*: A link signature is measured in state i while there exists in the history some other signatures of state i, however, the new measurement is far enough away from the measurements

---

[3]The measurement set used in Figure 7 did not have enough measurements to determine the Markov chain parameters.
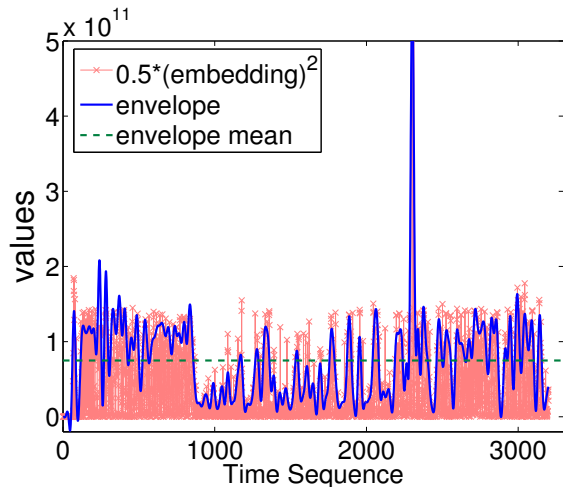

Figure 9: Squared 1D embedding coordinates and the envelope

Location	π_1	π_2	P_{12}	P_{21}
LOCA	0.5030	0.4970	0.0170	0.0168
LOCB	0.8562	0.1438	0.0256	0.0043
LOCC	0.5272	0.4728	0.0126	0.0113
LOCD	0.5678	0.4322	0.0402	0.0306

Table 2: Probabilities of states and transitions at four different locations.

in the history that they are detected as different, thus a false alarm is raised.

2. *Different-State False Alarm(DSFA)*: A link signature is measured in state i, but no signature previously measured in state i exists in the history. Because link signatures from states $j \neq i$ are very different from those measured in state i, this new measurement does not match any in the history, and a false alarm is raised.

As in Section 4, we store a finite history of links signatures for each link. Let N be the total buffer size for saving this history of link signatures of a link across all states. Every time we record a new link signature, to place it in the history, it must replace one of the existing measurements in the history. In this paper, we compare two buffer replacement policies:

- *Policy 1*: The history has a first-in first-out (FIFO) replacement policy. The new measurement replaces the oldest measurement in the history. Policy 1 is the policy that was considered by [11].

- *Policy 2*: The history is subdivided into K separate FIFO buffers, one for each state in the Markov chain. When a new measurement is made, we estimate to which state it belongs, and it replaces the oldest measurement within that state's buffer.

Other replacement policies are also possible but we do not evaluate those in this paper. Here, we show how Policy 1 and Policy 2 differ in the probability of a DSFA.

First, consider Policy 2. Assuming that each state's buffer is initialized with some measurements from that state, when

a new link signature is measured from any of the K states, it cannot experience a DSFA. This is by definition, since the DFSA occurs only when in a state for which no past link signatures exist in the history. Since Policy 2 keeps some measurements from each of the K states, this will not happen, as long as we have previously established the K possible states which the link may experience.

In contrast, consider Policy 1. Since the history does not discriminate between link signatures measured at different states, it is possible that FIFO buffer will not currently hold at least one measurement from each of the K states. In this case, if the Markov chain travels to a state without any measurements in the FIFO buffer, then the new measurement will trigger a DSFA. In this section, we quantify the probability of DFSA when using Policy 1. Because the probability of DFSA under Policy 2 is zero, this section quantifies the improvement in the false alarm rate. This improvement, in Policy 2, is achieved by making the replacement policy better matched to the physical model underlying the changes over time experienced by link signatures.

In this paper, we attempt to eliminate DSFAs by dividing the single N-length FIFO into K FIFOs each with length N/K. While in state i, the receiver will insert measured link signatures into FIFO i. To calculate the probability of DFSA using Policy 1, we note that the DFSA error occurs when the Markov chain enters state i when all link signatures in the history were to be measured outside of state i. We then use analysis of Markov chain models to calculate the probability of DSFA, first for the case of a $K = 2$ state Markov chain, and then for the general $K > 2$ case.

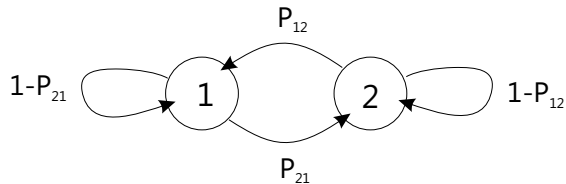### 6.2.2 Two-state Markov Chain Model

Figure 10: A 2-state Markov chain

For $K = 2$, we can exactly evaluate the probability of DFSA in Policy 1. Figure 10 shows a two-state Markov chain and its transition probabilities. It can be seen that the probability of DSFA given that we are entering state 1 is the probability that we started in state 2 N time units ago, and that we stayed in state 2 for N consecutive time units. Conversely, the probability of DSFA given that we are entering state 2 is the probability that we started in state 1 N time units ago, and stayed in state 1 for N consecutive time units. This means that,

$$P[\text{DSFA}] = \pi_2 P_{22}^N P_{12} + \pi_1 P_{11}^N P_{21} \qquad (21)$$

where $\pi_1 = P_{12}/(P_{21} + P_{12})$, and $\pi_2 = P_{21}/(P_{21} + P_{12})$.

6.2.3 $K > 2$ State Markov Chains

Generally we can use Markov chain models to analyze the probability of DSFA when using Policy 1. In particular, if we denote X_n to be the state at time n, then we define the time to return to state i (commonly called the *hitting time*),

$$T_i = \min_{n>0}\{X_n = i | X_0 = i\}, \qquad (22)$$

that is, the first time n when we return to state i given that we were at state i at time 0. A standard Markov chain theoretical result is that $E[T_i] = 1/\pi_i$. We are interested in particular about $P[T_i > N]$ – this is the probability upon return to state i that we will have a DSFA error. While the exact probability is difficult to write in general, we can generally approximate it for large N. For this, we assume that the tail of the probability mass function (pmf) of T_i is geometric. (This is exact in the $K = 2$ case.) The complementary CDF of a geometric pmf with mean $1/\pi_i$ is

$$P[T_i > N] = (1 - \pi_i)^{N+1}.$$

Thus the probability of a DSFA, using the law of total probability, is

$$P[DSFA] = \sum_i \pi_i P[T_i > N] \approx \sum_i \pi_i (1 - \pi_i)^{N+1}. \quad (23)$$

6.3 Results

Using the link measurements described in Section 6.2, we have used this Markov chain analysis to compute the probability of DSFA as a function of the length N of the FIFO. We use the transition probabilities listed in Table 2, and calculate $P[DSFA]$ from (21). The results are given in Figure 11 for all four measured links. As we expect, the probability of DSFA decreases exponentially with the length of the history. However, if either factor $P_{22} = 1 - P_{12}$ or $P_{11} = 1 - P_{21}$ is very close to 1, the rate of convergence is very slow. In our measurements, these probabilities are in fact very close to one. At $N = 10$, the probability of DSFA is in the range of 0.6% to 2.5%, which are very significant error rates. Even with a history length $N = 100$, the DSFA is in the range of 0.11% to 0.36%. This high of a false alarm rate would likely be unacceptable to a user.
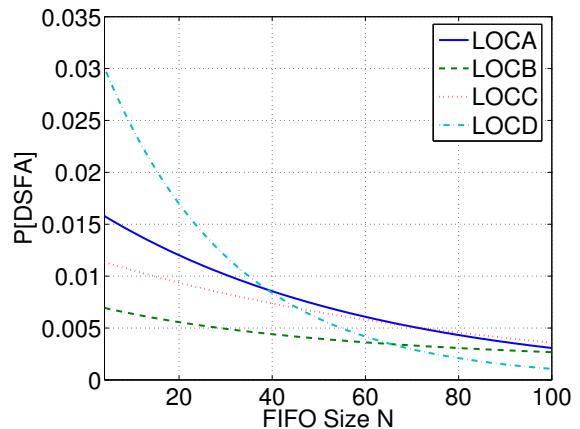

Figure 11: The probability of different-state false alarm (DSFA) for four different measured links.

By using Policy 2, as discussed above, we would see virtually no DSFA errors. The multiple FIFO buffers, each matched to a particular state, provide a reliable way to significantly reduce false alarms experienced by a location distinction algorithm. The accuracy of the temporal model is affected by the propagation environment. The measurements of this campaign are taken in an environment with moderate dynamics. In buildings with more motion such as shopping malls we expect more sophisticated models are

needed to obtain good distinction performance. We consider the further investigation in temporal modeling as one of our future works.

7. RELATED WORK

There has been a vast amount of research on localization or location estimation (e.g., [2, 9, 15, 14]). Unlike localization or location estimation, the objective of location distinction is only to distinguish one link signature from another, and not to map the signature to a particular physical coordinate. Localization techniques such as time of arrival (TOA), time difference of arrival (TDOA), and angle of arrival (AOA) may not be effective or efficient at discriminating locations. For instance, a TOA based localization can have the following two shortcomings. First, the transmitter may not be suitably synchronized with the receiver. Second, when only one receiver is employed the TOA based localization cannot uniquely determine the location of the transmitter. Location distinction schemes, such as ours, can alleviate or completely avoid these problems.

Faria *et al* [4] proposed using RSS-based signalprints to prevent impersonation in wireless local area networks. Although this method uses the RSS measure that is readily available in commodity wireless cards, it fails to capture the rich multipath characteristics of wireless channels. Patwari *et al* [11] proposed the use of temporal channel impulse response, that captures the multipath characteristics of wireless channels, as a link signature for location distinction. Li *et al* [6] proposed the use of complex channel gains by multitonal probes, that also captures multipath effects, for securing wireless systems. Our work enhances the existing work on location distinction using link signatures in the following significant ways. First, we compare the two multipath-based scheme both qualitatively and quantitatively. No such comparison has been made in the existing work. Second, we enhance the Li [6] method with a new metric. Third, we develop a new link signature based on the strengths of the two multipath-based schemes. We also, very importantly, measure and develop a Markov chain model for the temporal behavior of link signatures and integrate this model in our location distinction mechanism.

There is a growing interest in exploiting physical characteristics of wireless channels for network security (e.g., [1, 7]). Although security is one application area in which our link signature measurements and location distinction mechanisms can be applied, the contributions of this paper are more general than addressing a specific security threat. The application of our location distinction methodology to specific security scenarios will be an interesting enhancement of our research.

8. CONCLUSIONS

In this paper, we compared two existing multipath-based location distinction methods. We also improved the multiple tone probing method. We then used the strengths of the two existing methods to develop a new link signature. Our extensive measurement results showed that the new link signature consistently outperforms the existing signatures even after the existing signatures are enhanced with our proposed improvements. We performed a measurement campaign to understand and model the temporal behavior of link signatures. We integrated our model in our location distinction

mechanism to reduce the probability of false alarms. In the future, we plan to apply our methodology to more data sets. We also propose to build our methodology on the GNU radio platform. We believe that link signatures will continue to evolve especially with the development of SDR [8, 3, 13], ultra-wideband, and other new wireless technologies.

9. REFERENCES

[1] B. Azimi-Sadjadi, A. Kiayias, A. Mercado, and B. Yener. Robust key generation from signal envelopes in wireless networks. In *CCS '07: Proceedings of the 14th ACM conference on Computer and communications security*, pages 401–410, New York, NY, USA, 2007. ACM.

[2] P. Bahl and V. N. Padmanabhan. RADAR: an in-building RF-based user location and tracking system. In *IEEE INFOCOM 2000*, pages 775–784, 2000.

[3] V. Bose, M. Ismert, M. Wellborn, and J. Guttag. Virtual radios. *IEEE JSAC*, 17(4):591–602, April 1999.

[4] D. B. Faria and D. R. Cheriton. Radio-layer security: Detecting identity-based attacks in wireless networks using signalprints. In *Proc. 5th ACM Workshop on Wireless Security (WiSe'06)*, pages 43–52, Sept. 2006.

[5] S. M. Kay. *Fundamentals of Statistical Signal Processing*. Prentice Hall, New Jersey, 1993.

[6] Z. Li, W. Xu, R. Miller, and W. Trappe. Securing wireless systems via lower layer enforcements. In *Proc. 5th ACM Workshop on Wireless Security (WiSe'06)*, pages 33–42, Sept. 2006.

[7] M. G. Madiseh, M. L. McGuire, S. W. Neville, and A. A. B. Shirazi. Secret key extraction in ultra wideband channels for unsynchronized radios. In *6th Annual Conference on Communication Networks and Services Research (CNSR2008)*, May 2008.

[8] J. Mitola. The software radio architectuer. *IEEE Communications Magzine*, 33(5):26–38, May 1995.

[9] L. M. Ni, Y. Liu, Y. C. Lau, and A. P. Patil. Landmarc: indoor location sensing using active rfid. *Wirel. Netw.*, 10(6):701–710, 2004.

[10] N. Patwari and S. K. Kasera. CRAWDAD utah CIR measurements. http://crawdad.cs.dartmouth.edu/meta.php?name=utah/CIR.

[11] N. Patwari and S. K. Kasera. Robust location distinction using temporal link signatures. In *ACM Intl. Conf. on Mobile Computing Networking (Mobicom'07)*, Sept. 2007.

[12] J. B. Tenenbaum, V. de Silva, and J. C. Langford. A global geometric framework for nonlinear dimensionality reduction. *Science*, 290:2319–2323, Dec 2000.

[13] D. L. Tennenhouse and V. G. Bose. A software-oriented approach to wireless signal processing. In *Mobile Computing and Networking*, pages 37–47, 1995.

[14] K. Whitehouse, C. Karlof, and D. Culler. A practical evaluation of radio signal strength for ranging-based localization. *SIGMOBILE Mob. Comput. Commun. Rev.*, 11(1):41–52, 2007.

[15] K. Yao and F. Lorenzelli. Localization in sensor networks. *ST Journal of Research*, 4(1):80–96, 2007.